TRANSONIC AFTERBODY SIMULATION
ATAC – TEST CASE 1D

Alexander Filimon, Heinrich Luedeke
DLR, Institute of Aerodynamics and Flow Technology
Lilienthalplatz 7, D-38108 Braunschweig

1. Introduction

One challenge of numerical investigations of unsteady super- and hypersonic flow fields is the study of turbulent wake flow and the interaction with nozzle sections at modern launcher configurations. Unsteady side-loads, induced by the interaction of flow separation inside of the nozzle and the launcher wake will strongly influence the design of future main stage propulsion systems. This interaction phenomenon, called buffeting coupling, is one of the main challenges during ascent. The purpose of the presented study is to simulate a combined generic base-flow nozzle configuration as shown in Fig. 1 under fully turbulent conditions (see also [1]). It is intended as a generic model of the central stage of a launcher, including central body and nozzle area. Experimental data under transonic conditions is available from wind tunnel tests in the scope of the ATAC program. Simulations are carried out with recent turbulence models like detached-eddy simulation (DES). DES is a hybrid technique proposed by Spalart et.al. for the simulation of this kind of turbulent unsteady flows. The idea is to combine the best features of Reynolds-averaged Navier-Stokes (RANS) and the large eddy simulation (LES) for the computation of realistic configurations at high Reynolds numbers.
The study was carried out by means of unstructured grids in the whole area including jet- and nozzle flow. Special care was taken on the influence of the time step size on the unsteady results and on grid influences. Comparisons with experimental pressure data, RMS distributions and power spectra have shown good agreement with the predicted DES results.

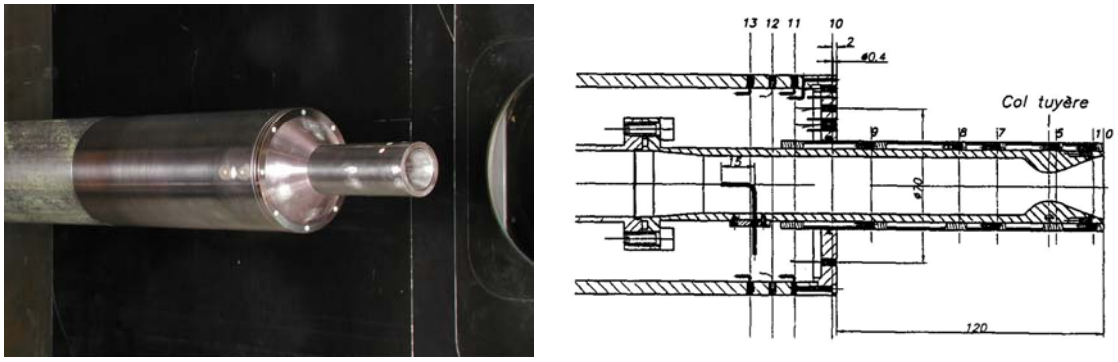

Fig. 1 Investigated configuration in the wind tunnel and construction drawing

2. Numerical tools

The presented investigation was carried out by the hybrid structured/unstructured DLR-Navier-Stokes Solver TAU, which is validated for a wide range of steady and unsteady sub- trans- and hypersonic flow cases [2].
The advantage of a hybrid code is to combine the superior quality of structured grids to resolve wall heat transfer or wall shear stress with the ability of unstructured grids to efficiently resolve flow regions of particular interest.
TAU is a second order finite-volume flow solver for the Euler and Navier-Stokes equations in the integral form. Different numerical schemes like cell-centred for sub- and transonic flow and AUSMDV for super- and hypersonic flow conditions are implemented. Second-order accuracy for upwind schemes is obtained by the MUSCL extrapolation, in order to allow the capturing of strong shocks and contact discontinuities. A three-stage Runge-Kutta scheme is used to advance the solutions in time for steady flow fields. For acceleration of the convergence local time stepping, implicit residual smoothing and full multigrid are optional.

For fast and accurate transient flow simulations a dual time stepping scheme, following Jameson is implemented, which is an implicit algorithm and not restricted in the choice of the smallest timestep in the flow field. To overcome this limit the time derivative in the Navier-Stokes equations is discretized by a second order backwards difference, resulting in a non-linear equation system which converges towards the subsequent timestep by using an inner pseudo-time. Within this inner loop all mentioned acceleration techniques such as local time stepping and residual smoothing are applicable. With this approach an acceleration of time accurate calculations of 2nd up to 3rd order is possible.
Several one- and two equation turbulence models are available for steady simulations. In the presented RANS-cases the one-equation Spalart-Allmaras (SA) model is used which is described detailed in [3].
During the last years more recent turbulence models like DES are implemented [4],[5]. DES is a hybrid RANS-LES approach that bases on a modification of the wall distance term in the SA model [6]. While RANS is used in the unsteady boundary layer flow where it performs reasonable results, LES is used in separated regions where relevant turbulent scales can be modelled. The switching between RANS and LES bases on a characteristic length scale, chosen to be proportional with Δ which is the largest cell dimension:

$$\Delta = \max(\Delta x, \Delta y, \Delta z) \tag{6}$$

For the standard DES formulation the wall distance d in the SA model is replaced by $\tilde{d}$ where $\tilde{d}$ is defined as:

$$\tilde{d} = \min(d, C_{DES}\Delta) \tag{7}$$

with C_{DES} as a constant calibrated by using isotropic turbulence. In this mode a local equilibrium between production and destruction term in the SA model is expected. This local balance leads to the relation $\tilde{\nu} \propto \tilde{S} \cdot \tilde{d}^2$ with $\tilde{\nu}$ as the modified eddy viscosity in the Spalart-Allmaras model and $\tilde{S}$ as a modified vorticity similar to the relation of the Smagorinsky LES model.

3. Grid and flow conditions

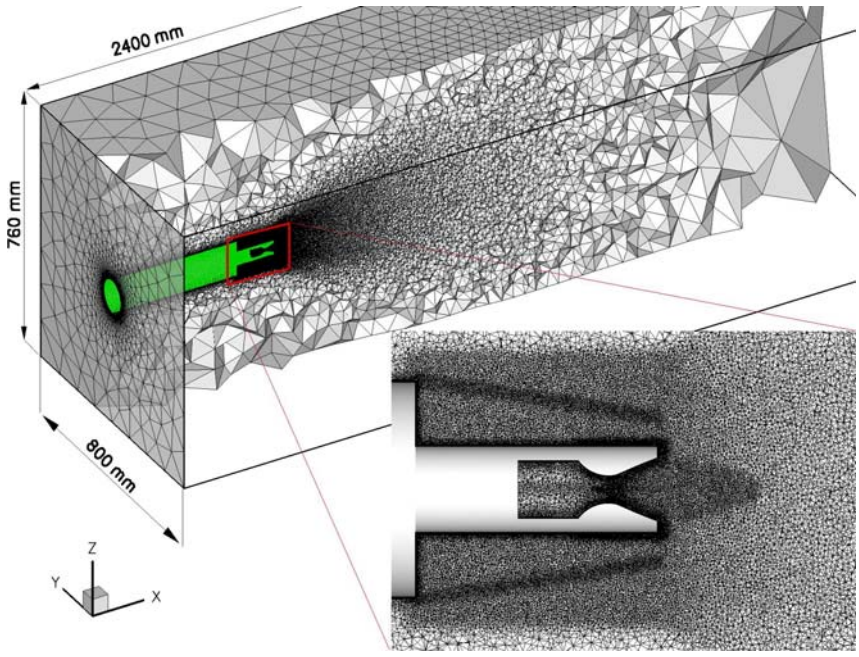

Fig. 2 Unadapted grid for nozzle-baseflow configuration.

The investigated test case was simulated under transonic conditions of Mach 0.7 at a nozzle pressure ratio pc/pa of 34.7 which means over expanded nozzle conditions without separation, cold gas conditions of 300 K in the thrust chamber and 312 K ambient temperature where expected. A fully turbulent flowfield was investigated due to a Reynolds number of $14.4 \cdot 10^6$.
Different unstructured grids are generated for the configuration. The basic grid is shown in Fig. 2.

It is pre-refined in the critical regions to resolve at least roughly all physical effects and to keep the ability to be adapted in further steps for the respect application. This was especially necessary for the shock system as shown in Fig. 3. For a better resolution of shear instabilities further improved grids are generated, which will be described later on.

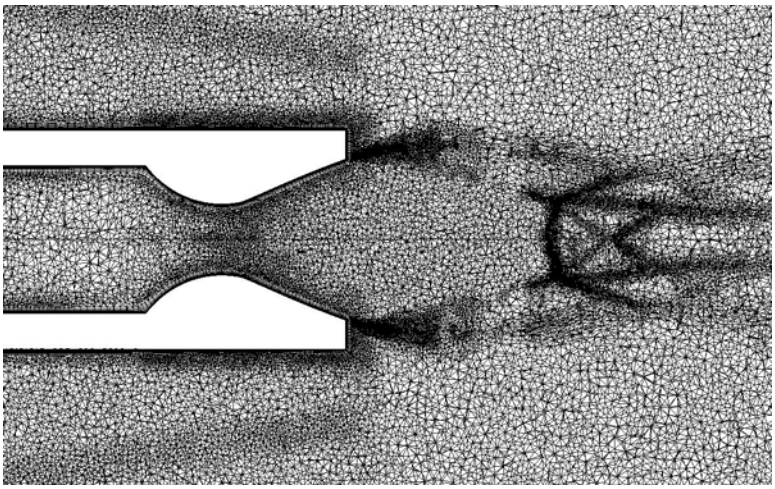

Fig. 3 Adapted grid in the nozzle region.

4. Steady RANS Simulation

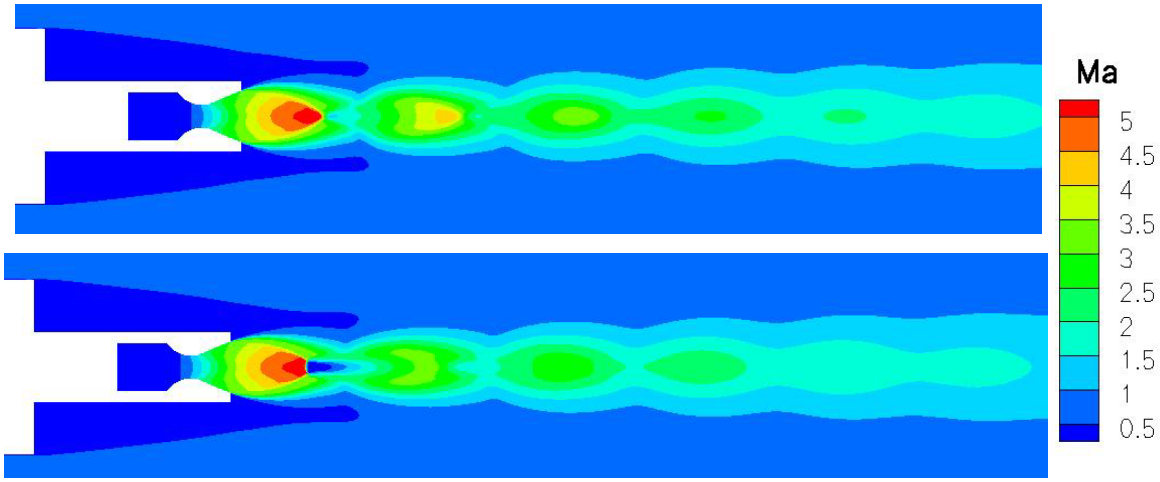

Fig. 4 Mach number distribution in the jet. Top: without adaptation, bottom: adapted.

As a first step, steady RANS simulations of the flow field, and especially of the jet, where carried out on the basic grid, as described in the former section. As visible in Fig. 4 the main flow field pattern in the plume, as well as the flow topology is well reproduced. Nevertheless important details like the mach disk behind the nozzle are missed, since a much higher resolution of the grid would be necessary in such regions. To capture these structures the tetrahedral grid was adapted in the jet region. This results in an improvement of the shock resolution as expected, also due to improved expansion angle. Changes in the wake flow are only marginal.

5. Time step study

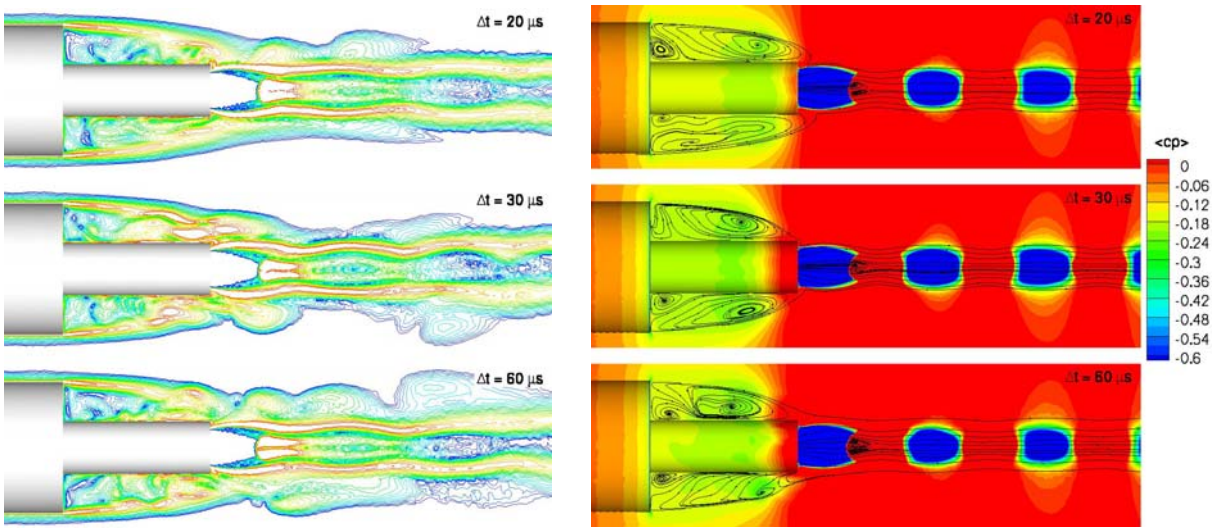

Fig. 5 DES simulation with different time step size. Left: vorticity contours, right: averaged pressure contours and stream traces.

Detached eddy simulations are carried out for different time steps to investigate the influences of appropriate time resolution on the resolution of the turbulence. Variations were done in a range, where the steps are all in an appropriate range for the separated transonic part behind the large cylinder. Particularly three time steps: 20, 30 and 60 µs are tested. The resulting snapshots of the vorticity on the left hand side of Fig. 5 show a smoothing out of turbulent structures in the shear layer as well as in the separated region for time steps of 20 and 60 µs. This can be explained by the additional numerical dissipation, inserted by the implicit scheme, which can be minimized by an appropriate time step. It increases for smaller time steps since more iterations of the dual time stepping are necessary as well as for larger ones since higher frequencies are not resolved.
From this variation also effects on the averaged simulated flow field are demonstrated in Fig. 5 on the right hand side where the averaged C_p distribution and stream lines are compared. Significant changes of the reattachment and secondary separations at the connection edge between large and small cylinder result from the different time steps.

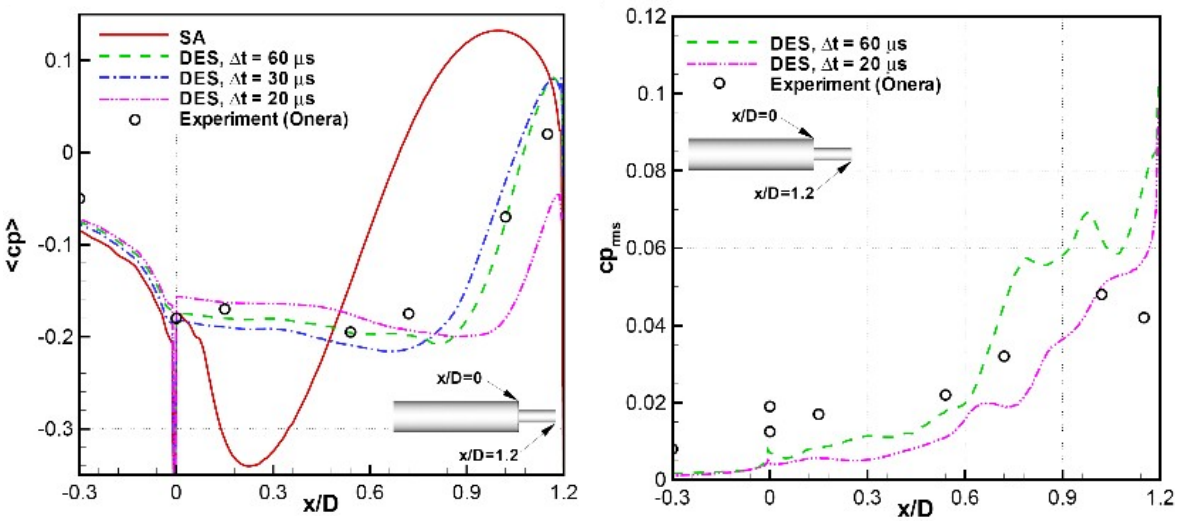

Fig. 6 Statistical data from DES results with different time steps. Left: averaged C_p distribution along the cylinder surface, right: RMS value of C_p.

6. Simulations on adjusted grid

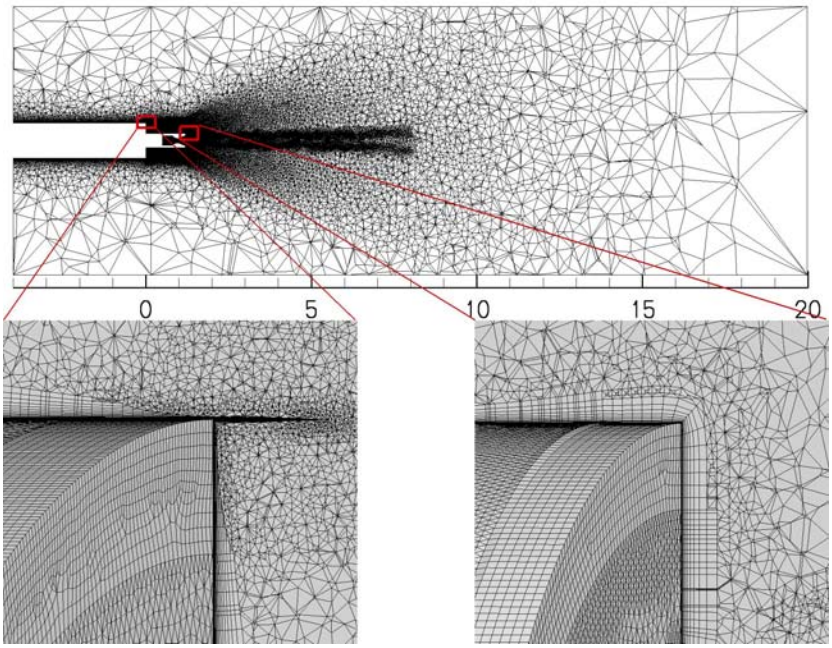

Fig. 7 Grid improvement by hexahedral boundary layer and refinement of the shear layer near the trailing edge of the large cylinder.

It was shown in former studies, that the fine resolution of the region where instabilities are first generated in the shear layer are a crucial point for the quality of transient turbulent simulations. To guarantee a high level of accuracy in this part of the flow field strongly refined grids as well as hexahedral parts in the boundary layer are chosen. A disadvantage of the chosen technique is the chopping of prismatic cells in the beginning shear layer, which is a restriction of the grid generator CENTAUR that slightly decreases the level of accuracy.

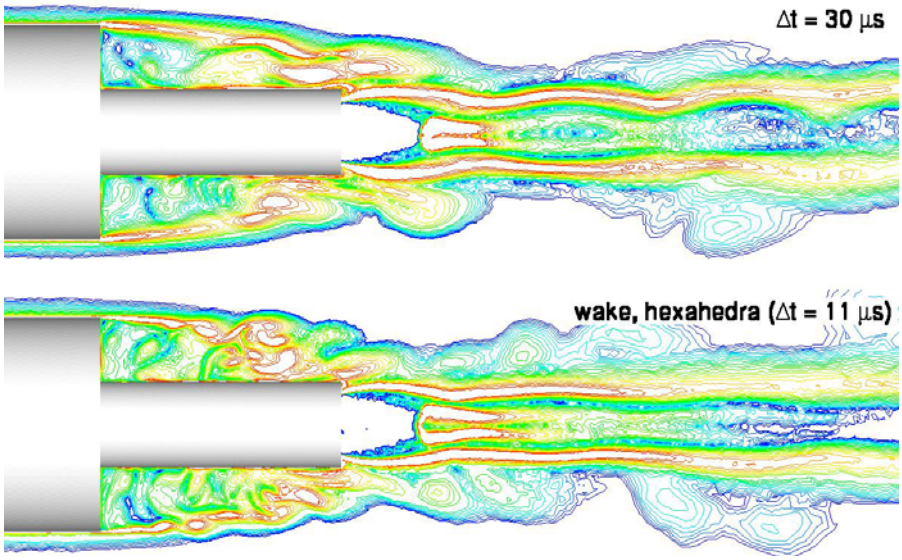

Fig. 8 comparison of shear layer resolution on different grids. Top: standard grid, bottoms: grid with hexahedral wake.

A first comparison of the results on tetrahedral and new grid by the vorticity in a snapshot (Fig. 8) give an impression of the improvements introduced by the new discretization. While in the upper figure the shear layer instabilities increase slowly down to the end of the small cylinder, the turbulent structures in the lower figure are much smaller and better resolved.

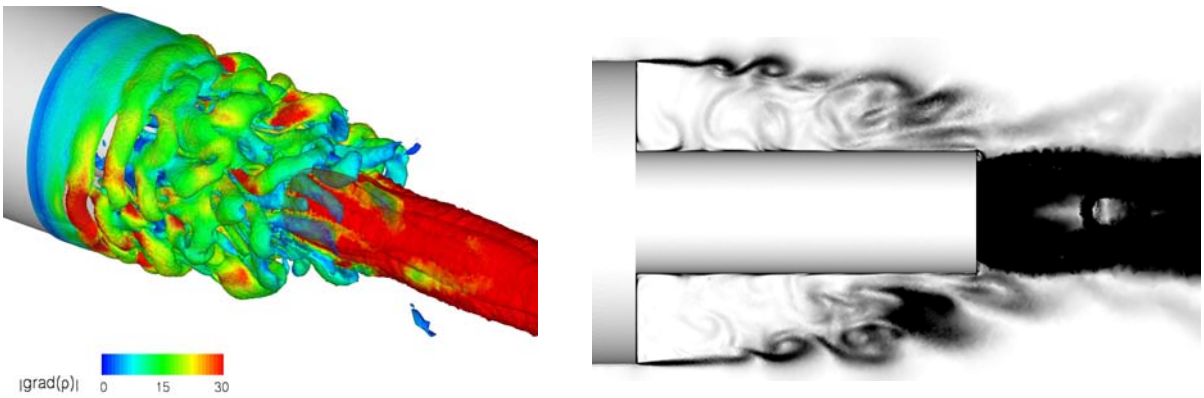

Fig. 9 Left: Q-criterion coloured by the density gradient in the wake flow on the improved grid. Right: schlieren type visualization of the density gradient in the symmetry plane.

The same tendencies can be visualized by the Q-criterion ($Q = 0.5 \cdot (\Omega_{ij} \cdot \Omega_{ij} - S_{ij} \cdot S_{ij})$) which is a good indicator for turbulent structures (Fig. 9 left), as well as by the density gradient as a numerical schlieren picture (Fig. 9 right). Although the averaged pressure along the smaller cylinder is overestimated, as well as the RMS values of Cp (Fig. 10), the shape of the distribution is by far better fitted and especially the position of the maxima agrees well with the experimental data.

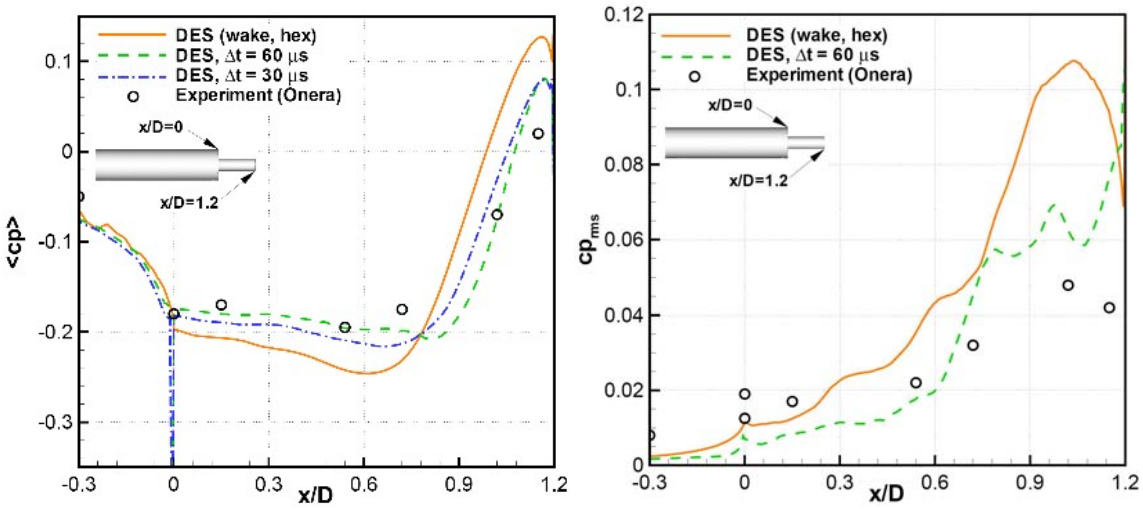

Fig. 10 averaged pressure along cylinder and RMS values of the pressure.

7. Statistics and Power Spectra

Finally on the improved grid also the directivity of the side loads is taken, as visible in Fig. 11. While the suction effect of the jet is still overestimated the isotropic character of the side loads is demonstrated successfully. Also the power spectra of fixed points are derived from the simulations (Fig. 12). The distribution of the power spectra was calculated by means of the instructions to the contributors by Philippe Meliga. Although the time series of 40ms used for the spectra need a longer sample to get a smooth spectrum, in both cases the well known peak at Strouhal number 0.2 and a lower peak at 0.1 as well as higher frequency bands near the re-attachment point are found.

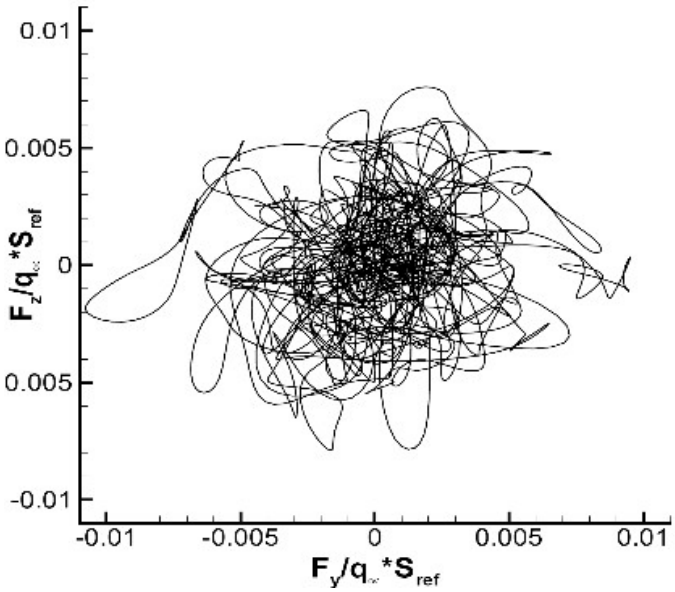

Fig. 11 directivity of the loads, calculated with jet.

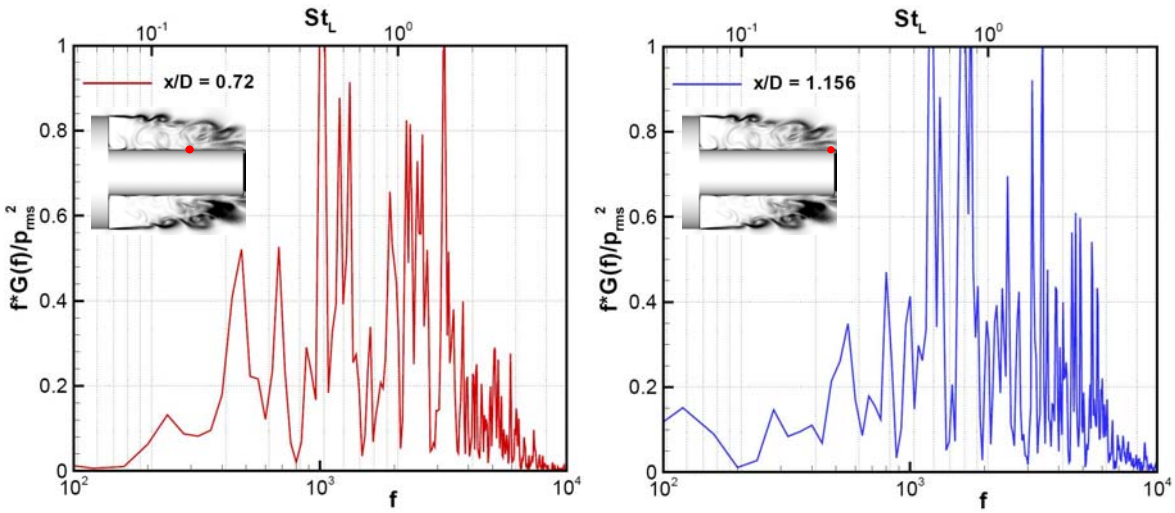

Fig. 12 Power spectral density of the pressure distribution at two different positions.

8. Conclusion

For the current study a combined base- and nozzle flow under transonic conditions was simulated by detached eddy simulation. Time convergence studies with different time step sizes were investigated. It was shown, that a hexahedral discretization of both both cylinder trailing edges leads to a better resolution of the onset of instabilities at the beginning of the shear layer in the wake. By this technique and a sufficient refinement a good resolution of turbulent structures behind the base could be demonstrated. Although the absolute level of the maximum pressure amplitudes is overpredicted, the location of this maximum fits quite well with the experimental data. Also the frequency level derived from the time series at different locations fits with the experimental data published in former studies.

References

[1] S. Deck, P.Guillen: Numerical Simulation of Side Loads in an Ideal Truncated Nozzle. 14th Journal of Propulsion and Power, Vol. 18, No. 2, 261-269 (2002).

[2] A. Mack, V. Hannemann: Validation of the unstructured DLR-TAU-Code for Hypersonic Flows, AIAA 2002-3111, (2002).

[3] P.R. Spalart, S.R. Allmaras: A One Equation Turbulence Transport Model for Aerodynamic Flows, La Recherche Aérospaciale, No. 1, 1994, pp. 5-21.

[4] H. Lüdeke, A. Filimon: Investigations of Transient Flow Phenomena at the ARIANE-5 Propulsion System During Ascent. 5th European Symposium on Aerothermodynamics for Space Vehicles, Cologne, November 8-11 (2004).

[5] H. Lüdeke, A. Filimon: Time Accurate Simulation of Turbulent Nozzle Flow by the DLR TAU-code. 14th DGLR (SRAB) STAB Symposium, Bremen, November 16-18 (2004).

[6] P.R. Spalart: Young-Person's Guide to Detached- Eddy Simulation Grids. NASA/CR-2001-211032, (2001).